

Experimental and theoretical study of spontaneous spin polarization and hysteresis in cesium vapor

A. Andalkar,* R. B. Warrington,† M. V. Romalis, S. K. Lamoreaux,‡ B. R. Heckel, and E. N. Fortson§
Department of Physics, Box 351560, University of Washington, Seattle, Washington 98195-1560

(Received 8 August 2001; published 11 January 2002)

We report results of measurements and theoretical modeling of spontaneous spin polarization and associated hysteresis in an optically pumped Cs vapor. We observe hysteresis over the full range (20–450 torr) of N_2 buffer gas pressures tested, and on two hyperfine components of the $D1$ transition, so long as both electronic spin exchange and optical pumping of a resolved ground state hyperfine level take place faster than spin relaxation. On the $F=3 \rightarrow F_e=4$ transition, the spin angular momentum is gained from the linearly polarized pump light, while on the $3 \rightarrow 3$ transition, it comes instead from the buffer gas during collisional quenching. The density-matrix theoretical model we have developed includes the effects of coherence in the excited state. It reproduces all observed features of spontaneous polarization, including hysteresis curves in quantitative agreement with the data across a broad range of experimental parameters.

DOI: 10.1103/PhysRevA.65.023407

PACS number(s): 32.80.Bx, 42.65.Pc, 34.10.+x

I. INTRODUCTION

Under certain conditions, an alkali-metal vapor illuminated with unpolarized or linearly polarized light can spontaneously develop a large spin polarization [1,2]. When the rates of electronic spin exchange and optical pumping of a resolved ground-state hyperfine level sufficiently exceed the rate of spin relaxation, the state of zero spin polarization becomes unstable, and any small initial bias grows exponentially into either of the two stable states with a large spin polarization parallel or antiparallel to an applied magnetic field. The atomic spin polarization then displays striking hysteresis in switching between the bistable states as the degree of circular polarization of the pumping light is varied across zero (see Fig. 1). By contrast, in normal optical pumping the spin polarization is proportional to the degree of circular polarization of the light along the magnetic field, and is zero for linearly polarized light.

Following an early prediction [1], the first observation of spontaneous polarization was made in cesium vapor on the $F=3 \rightarrow F_e=4$ hyperfine component of the 894 nm $D1$ line [2].¹ Here we report much more extensive observations of spontaneous polarization in cesium vapor, together with the development of an atomic theory of the process that predicts hysteresis curves in excellent agreement with observations. We find that spontaneous polarization, far from being confined to a narrow region of parameter space, is a surprisingly robust effect that takes place over wide ranges of cesium density, buffer gas pressure, and pump laser intensity, wavelength, and polarization. Spontaneous polarization strong

enough to produce hysteresis has been observed over the full range (20–450 torr) of N_2 buffer gas pressures tested (Fig. 1) and at temperatures ranging from 60–120 °C (Cs densities of 10^{12} to 5×10^{13} cm^{-3}). Of particular interest, we report the observation of spontaneous polarization on the $3 \rightarrow 3$ hyperfine component, in which the spin angular momentum is extracted not from the pump light but from the N_2 buffer gas molecules during collisional quenching. We have also observed evidence of the spontaneous, bistable nature of the phenomenon, whereby under identical experimental conditions the atomic ensemble may develop into either of the two bistable spin-polarized states during repeated trials.

In Sec. II we give a brief, qualitative discussion of the mechanism of spontaneous polarization, followed by a more detailed theoretical treatment in Sec. III. This density-matrix treatment includes the effect of coherence in the excited state, which is important when the excited-state hyperfine

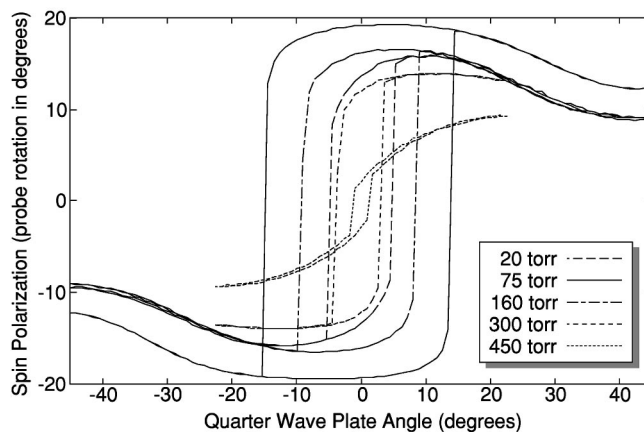


FIG. 1. Experimental hysteresis curves due to spontaneous polarization, for pumping on the $3 \rightarrow 4$ hyperfine component of the Cs $D1$ transition at N_2 buffer gas pressures of 20–450 torr. The horizontal axis is a measure of the circular polarization of the pump light, of which only a small component lies along the magnetic field. See Sec. V for discussion.

*Electronic address: andalkar@u.washington.edu

†Present address: CSIRO Telecommunications and Industrial Physics, Lindfield NSW 2070, Australia.

‡Present address: Los Alamos National Laboratory, Los Alamos, NM 87545.

§Electronic address: fortson@phys.washington.edu;

<http://www.phys.washington.edu/~fortson/>

¹A possible mechanism for spontaneous nuclear spin polarization in optically pumped solids has been discussed in Ref. [3].

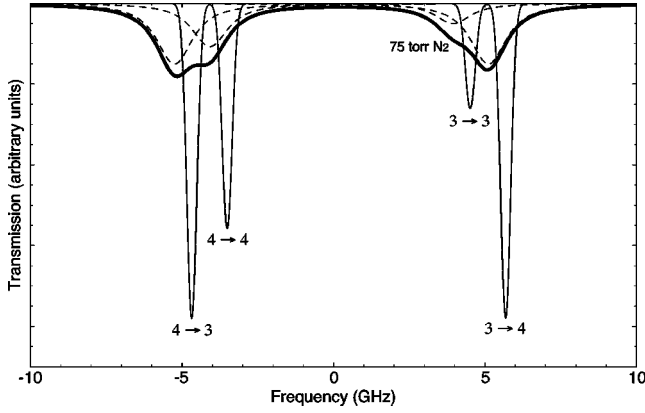


FIG. 2. Calculated hyperfine spectrum for the Cs $D1$ transition, showing transmission at 85°C for cells with 0 torr (thin line) and 75 torr (bold, with components shown dashed) of N_2 buffer gas. The hyperfine splitting is 9.2 GHz for the $6S_{1/2}$ ground state and 1.2 GHz for the $6P_{1/2}$ excited state. At 85°C , the Doppler width is about 400 MHz. The Lorentz full-width due to pressure broadening has been recently measured to be 19.5 MHz/torr for the Cs $D1$ transition in N_2 buffer gas [4], or about 1.5 GHz at 75 torr.

levels are only partially resolved. In Secs. IV and V we discuss the experimental apparatus and the major types of data collected, and then quantitative comparisons between the experimental data and the predictions of the theoretical model are made in Sec. VI.

II. BASIC MECHANISM

We begin with a qualitative discussion of the basic mechanism of spontaneous polarization, which involves three processes: optical excitation, collisional quenching with a buffer gas, and spin-exchange repopulation of the pumped ground-state level. In the Cs atom (nuclear spin $I=7/2$), the $6S_{1/2}$ ground state and $6P_{1/2}$ excited state are each split into two hyperfine levels of total angular momentum $F=I\pm 1/2=3$ and 4 (see Fig. 2). A magnetic field \mathbf{B} is applied, large enough that the Larmor frequency is greater than the pumping and spin relaxation rates, though not so large that the Zeeman splitting is resolved optically. In all cases of spontaneous polarization observed thus far, the pumping light excites a resolved $F=3$ hyperfine level, leaving the $F=4$ level relatively unpumped.

In spontaneous polarization, an imbalance of transition probabilities (Clebsch-Gordan coefficients) among the magnetic substates leads to a net amplification of the atomic spin polarization. For optical excitation on the $3\rightarrow 4$ transition, spontaneous polarization is maximized when the pump light is linearly polarized perpendicular to \mathbf{B} . In this case, the magnetic quantum number m along \mathbf{B} must change by $\Delta m = \pm 1$ during excitation. For an $F\rightarrow F+1$ transition, $|m|$ is more likely to increase than decrease [see Fig. 3(a)]. Thus, any initial ensemble-averaged polarization magnitude $\mathcal{M} \equiv |\langle m \rangle|$ will increase, with the extra angular momentum extracted from the pump light. Such an initial population bias may arise from a small applied circularity of the pump light, or from statistical fluctuations alone if experimental biases are sufficiently reduced (see Sec. V).

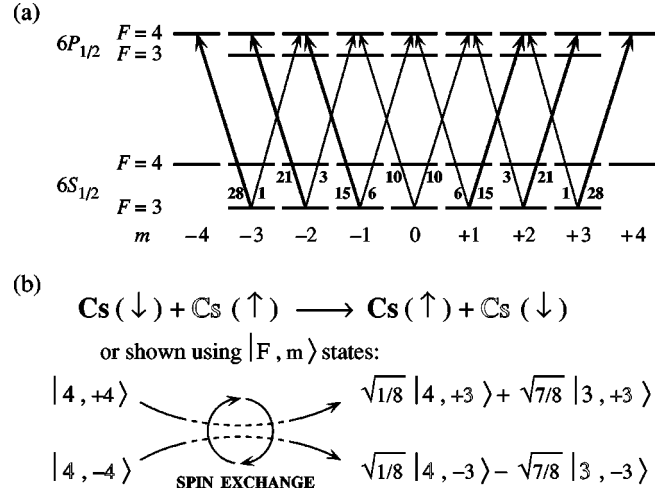


FIG. 3. (a) Polarization gain during excitation on the $3\rightarrow 4$ component. Relative transition rates from each of the m substates of the $F=3$ ground-state hyperfine level are shown, for pump light linearly polarized perpendicular to \mathbf{B} . From any nonzero m substate, $|m|$ is more likely to increase than decrease. This imbalance leads to a net increase of any bias in atomic polarization $\langle m \rangle$. (b) Example illustrating that electronic spin exchange repopulates the pumped $F=3$ level from the $F=4$ while preserving $\langle m \rangle$, thus completing the pumping cycle. The vertical arrows indicate electron spin direction, and the solid and outline fonts distinguish the two cesium atoms.

Collisional quenching of the excited-state Cs atoms then repopulates the ground state without emitting any light, which by reabsorption would tend to depolarize ground-state atoms. The loss in \mathcal{M} during quenching is, on average, less than the gain during pumping. Assuming that quenching repopulates the m sublevels in the same proportion as spontaneous radiation, the net increase in \mathcal{M} over a complete cycle is $\Delta\mathcal{M} = |\langle m(25-m^2)/6(m^2+20) \rangle_3|$, with the subscript denoting an average taken over all starting substates m in the $F=3$ level. We use N_2 buffer gas in the cell, since it has a large cross section ($\approx 80 \text{ \AA}^2$) for quenching the $6P_{1/2}$ and a much smaller cross section ($\approx 5 \text{ \AA}^2$) for changing the $6P_{1/2}$ to the more readily depolarized $6P_{3/2}$ [5].

Spin exchange completes the pumping cycle. Atoms which have been quenched to the $F=4$ level are brought back to the pumped $F=3$ level by electronic spin exchange with other ground-state Cs atoms. These spin-exchange collisions can change F but always preserve \mathcal{M} [6], as shown in Fig. 3(b). Another pumping cycle then begins, and spin polarization continues to build up. In the ideal case with no spin relaxation, the only two stable states are those with all atoms in the ground-state $F=4$ with $m = \pm 4$, i.e., all of the spins aligned parallel or antiparallel to \mathbf{B} . Spin relaxation reduces the degree of spin polarization from the ideal case, so that $\mathcal{M} < 4$ for either of the bistable states.

For the case of pumping on the $3\rightarrow 3$ transition, spontaneous polarization occurs via a different mechanism. For this transition, it is optimal for the pump light to be linearly polarized parallel to \mathbf{B} , so that only transitions with $\Delta m = 0$ are permitted and there is no change in \mathcal{M} during the excitation. Then during collisional quenching, atoms which make a

$F \rightarrow F+1$ transition to the ground-state $F=4$ level will gain polarization, so that the net gain during transitions to all ground-state levels is $\Delta\mathcal{M} = |\langle m \rangle_3|/6$. In this case, $\Delta\mathcal{M}$ is extracted from the buffer gas rather than the pumping light. Spin exchange then repopulates the $F=3$ level without changing \mathcal{M} , just as in the earlier case.

At high buffer gas pressure, when the quenching rate exceeds the excited-state hyperfine frequency (but the much larger ground-state hyperfine splitting is still resolved), one need only consider the effect of optical pumping on the electron spin since \vec{J} decouples from \vec{I} in the excited state. Excitation of the $F=3$ level, in which \vec{J} is antiparallel to \vec{F} , leads to a net gain of $\Delta\mathcal{M} = |\langle m \rangle_3|/6$ in a complete pumping cycle for light linearly polarized perpendicular to \mathbf{B} .

Simple treatments of spontaneous polarization are possible when either the optical pumping rate or the spin-exchange rate dominates over all other rates [1,2]. Simple rate equations give the average polarization gain in one pumping cycle for each of the Cs $D1$ hyperfine components, as a function of the angle θ between the plane of polarization of the pump light and the magnetic field. In addition to the situations of positive gain outlined above, one also finds a positive gain on the $4 \rightarrow 3$ transition for small θ (although no attempt has yet been made to observe spontaneous polarization on this line). However, on the $4 \rightarrow 4$ transition the gain is strongly negative for all values of θ .

The negative gain on the $4 \rightarrow 4$ transition has important consequences for spontaneous polarization, since for most situations of experimental interest, the individual hyperfine components are broadened enough that the pump light is addressing more than one component simultaneously (see Fig. 2). For a given spontaneous polarization line, pumping on the wings of other lines, especially the $4 \rightarrow 4$ component, produces a significant depolarizing effect at moderate-to-high buffer gas pressures, which mimics the effects of a greater spin-relaxation rate and limits the regions where spontaneous polarization occurs. This produces the somewhat counterintuitive result that under conditions of spontaneous polarization the degree of atomic spin polarization does not increase indefinitely with pump power. As the pump power continues to increase, the negative gain due to pumping on other lines becomes the major source of spin relaxation and increases relative to the spin-exchange rate, until eventually spontaneous polarization fails to occur.

III. THEORETICAL MODEL

All of the basic mechanisms outlined above are contained rigorously in a theoretical model in which we numerically solve the general equations governing the time evolution of the ground-state density matrix $\rho_{gg'}$, with g denoting a ground-state sublevel $|nsJ_gF_gm_g\rangle$. The Larmor precession frequency about the applied magnetic field \mathbf{B} is assumed large enough that off-diagonal elements average to zero, so that the diagonal elements $\rho_{gg} = \rho(F_g, m_g)$ representing the population distribution over the Zeeman sublevels contain all the information about the ground-state atomic polarization. The rate of change of $\rho(F_g, m_g)$ can be written as the sum of three ground-state terms,

$$\dot{\rho} = \dot{\rho}_{\text{pump}} + \dot{\rho}_{\text{exch}} + \dot{\rho}_{\text{relax}} \quad (1)$$

for the optical pumping, electronic spin exchange, and spin-relaxation rates in the ground state.

Here, we outline our treatment of optical pumping. As is standard, we set $(\dot{\rho}_{gg})_{\text{pump}} = (\dot{\rho}_{gg})_{\text{depop}} + (\dot{\rho}_{gg})_{\text{repop}}$ to include both depopulation of the ground state by optical excitation and repopulation by collisional quenching [6]. Under the typical experimental conditions explored in this work, the hyperfine structure is well resolved in the ground state but only partially resolved in the excited state; it is thus necessary in repopulation to include the coherent effect of interference between transition amplitudes involving different hyperfine excited states. The pumped coherence among the excited sublevels is contained in the off-diagonal elements of the excited-state density matrix.

In a perturbation treatment, with all excited-state amplitudes small compared to ground-state amplitudes, the density-matrix equations describing the excitation of the atoms by monochromatic pump light of frequency ω are, in the interaction picture,

$$i\dot{\rho}_{gg} = \sum_e (\Omega_{ge} e^{-i\Delta\omega_{eg}t} \rho_{eg} - \Omega_{eg} e^{i\Delta\omega_{eg}t} \rho_{ge}), \quad (2)$$

$$i\dot{\rho}_{eg} = \Omega_{ge} e^{i\Delta\omega_{eg}t} \rho_{gg} + (\Delta\omega_{eg} - i\gamma_{eg}) \rho_{eg}, \quad (3)$$

$$i\dot{\rho}_{ee'} = \sum_g (\Omega_{eg} e^{i\Delta\omega_{eg}t} \rho_{ge'} - \Omega_{ge'} e^{-i\Delta\omega_{e'g}t} \rho_{eg}) + (\Delta\omega_{ee'} - i\gamma_{ee'}) \rho_{ee'}. \quad (4)$$

Here e is an excited-state sublevel $|npJ_eF_em_e\rangle$, Ω_{eg} the Rabi frequency of the pump light, $\Delta\omega_{eg} = \omega - \omega_{eg}$ the mistuning from resonance between sublevels g and e , $\Delta\omega_{ee'}$ the energy difference between two excited sublevels (zero if $e=e'$), γ_{ee} the rate at which atoms relax out of a given excited state (dominated by collisional quenching to the ground state by N_2 molecules), and γ_{eg} the total rate of relaxation of ρ_{eg} (which determines the homogeneous linewidth of the atomic absorption). $\gamma_{eg} = \gamma_{ee}/2 + \bar{\gamma}_{eg}$, with $\bar{\gamma}_{eg}$ the rate of dephasing between ground and excited states due to collisions, and $\gamma_{ee} \approx 0.25\gamma_{eg}$ (from Refs. [4,5]). All excited sublevels are assumed to have a common γ_{eg} and γ_{ee} , and consistent with the perturbation treatment, $|\Omega_{eg}| \ll \gamma_{ee}$. In Eq. (4) we have omitted collisional mixing and dephasing among excited-state sublevels, since for $J_e=1/2$, only negligible mixing should take place during the short time before quenching occurs. Also, we have omitted the small collisional transfer from $6P_{1/2}$ to $6P_{3/2}$. In the full model we include spin-relaxation terms to test for these effects.

The excited-state sublevels will quickly reach a quasi-steady state, with $\dot{\rho}_{eg} = \dot{\rho}_{ee} = 0$. Equations (3) and (4) then yield the steady-state solutions

$$\rho_{eg} \cong - \frac{\Omega_{ge}}{\Delta\omega_{eg} - i\gamma_{eg}} \rho_{gg}, \quad (5)$$

$$\rho_{ee'} \equiv \sum_g \frac{\Omega_{eg}\Omega_{ge'}}{\Delta\omega_{ee'} - i\gamma_{ee'}} \left[\frac{1}{\Delta\omega_{e'g} + i\gamma_{eg}} - \frac{1}{\Delta\omega_{eg} - i\gamma_{eg}} \right] \rho_{gg}. \quad (6)$$

Combining Eqs. (2) and (5), we obtain the following standard expression for the rate of depopulation of a ground state g :

$$(\dot{\rho}_{gg})_{\text{depop}} = - \sum_e \frac{2|\Omega_{eg}|^2}{\gamma_{eg}} \frac{\gamma_{eg}^2}{\Delta\omega_{eg}^2 + \gamma_{eg}^2} \rho_{gg}. \quad (7)$$

To reduce the Rabi frequency part of this equation to calculable form, we can write $2\hbar\Omega_{eg} = eE_0 \sum_q \langle e | \epsilon_q r_q | g \rangle$ with E_0 the electric-field amplitude of the pump light and ϵ_q the polarization components in a spherical basis. We then use standard expressions for decoupling angular momenta to obtain

$$\frac{2|\Omega_{eg}|^2}{\gamma_{eg}} = 3(2J_g + 1)\Gamma_0 \sum_q G_{geg}^q |\epsilon_q|^2, \quad (8)$$

where the general form of G when $g \neq g'$ is given by

$$\begin{aligned} G_{geg'}^q &= (2F_e + 1) \sqrt{(2F_g + 1)(2F_{g'} + 1)} \\ &\times \begin{pmatrix} F_g & 1 & F_e \\ -m_g & m_g - m_e & m_e \end{pmatrix} \begin{pmatrix} F_{g'} & 1 & F_e \\ -m_{g'} & -q & m_e \end{pmatrix} \\ &\times \begin{Bmatrix} J_g & 1 & J_e \\ F_e & I & F_g \end{Bmatrix} \begin{Bmatrix} J_{g'} & 1 & J_e \\ F_e & I & F_{g'} \end{Bmatrix}, \end{aligned} \quad (9)$$

in which I is the nuclear spin, and

$$\Gamma_0 = \frac{e^2 E_0^2}{2\hbar^2} |\langle J_e || r || J_g \rangle|^2 \frac{1}{3(2J_g + 1)\gamma_{eg}} \quad (10)$$

is the rate an unpolarized atom absorbs resonant light in the absence of hyperfine structure. In our case of interest, $J_e = J_g = 1/2$, and thus in summations over e (and later, g), only F and m vary.

The depopulation of ρ_{gg} in Eq. (7) is matched by repopulation from the pumped excited states. Excited states can act as virtual levels in the excitation/quenching process, or can be populated by real transitions made possible by the dephasing collisions. Both contributions are included in our treatment. We assume the quenching operator has equal amplitudes \mathcal{Q} distributed with random phases over all spatial orientations and all frequencies covering the spectrum of hyperfine components of the Cs $D1$ line. The repopulation of the ground state may then be written

$$(\dot{\rho}_{gg})_{\text{repop}} = \mathcal{N} \sum_{e,e'} \mathcal{Q}_{e'g} \cdot \mathcal{Q}_{ge} \rho_{ee'}, \quad (11)$$

where the normalization factor $\mathcal{N} = \gamma_{ee'} / (\sum_{\bar{g}} \mathcal{Q}_{\bar{g}e} \cdot \mathcal{Q}_{\bar{g}e'})$ includes a sum over the ground states (the dummy index \bar{g}) and is thus independent of e . \mathcal{Q} could, in principle, have both vector and scalar parts for a $J = 1/2 \rightarrow 1/2$ transition. In the

case of spontaneous decay by electric dipole radiation, \mathcal{Q} is a vector and can be set equal to \vec{r} . To describe collisional quenching by N_2 molecules, we include vector and scalar couplings in our full model [7], but find that a purely vector form for \mathcal{Q} is sufficient to account for our data. Using just the vector form here, substituting Eq. (6) into Eq. (11), and decoupling the angular momenta as above, we obtain the following expression for the total pump rate of the ground state,

$$\begin{aligned} (\dot{\rho}_{F_g, m_g})_{\text{pump}} &= 3(2J_g + 1)\Gamma_0 \sum_{q,e,e',g'} G_{geg'}^q G_{ge'e'}^q |\epsilon_q|^2 \\ &\times \frac{\gamma_{eg}\gamma_{ee'}}{\Delta\omega_{F_e F_e}^2 + \gamma_{ee}^2} \frac{\Delta\omega_{F_e F_e} \Delta\omega_{F_e F_{g'}} + \gamma_{eg}\gamma_{ee'}}{\Delta\omega_{F_e F_{g'}}^2 + \gamma_{eg}^2} \\ &\times [1 - \delta(g, g') \delta(e, e')] \rho_{F_{g'}, m_{g'}}, \end{aligned} \quad (12)$$

where Γ_0 and G are defined in Eqs. (9) and (10), and the delta functions inside the bracket give the depopulation term. Thermal motion, neglected for simplicity, may be included by Doppler convolution.

For the remaining terms in Eq. (1), $\dot{\rho}_{\text{exch}}$ and $\dot{\rho}_{\text{relax}}$, we use the density-matrix equations for ground-state electronic spin exchange and electronic spin relaxation given in Ref. [1]. We include ground-state relaxation due to both Cs-Cs [8] and Cs- N_2 collisions, and polarization loss due to diffusion to the cell walls [9,10]. As mentioned above, we also include a term for possible spin relaxation in the $6P_{1/2}$ excited state [11]. In addition, the model incorporates pump light propagation through the cell, including both the absorption and the change in the pump polarization state through the full complex susceptibility of the atomic vapor [12,13]. This propagation scheme accounts for the varying susceptibility as the degree of atomic spin polarization changes farther into the cell.

IV. EXPERIMENTAL APPARATUS

The experimental apparatus used to observe spontaneous polarization is shown in Fig. 4. The Cs vapor and N_2 buffer gas are contained in a 2.5 cm diameter, 2.5 cm long Pyrex cell, which is held within an oven. The Cs density and spin-exchange rate are set by adjusting the temperature of the cell. The magnetic field \mathbf{B} , typically about one gauss, lies in the xz plane at an angle α relative to the pump beam propagation direction z . In practice, α is typically quite large (around 80°) to avoid inducing a large degree of circularity due to absorption of the pump beam, which would tend to depolarize atoms farther into the cell. A set of three-axis Helmholtz coils outside the oven sets the magnitude and direction of \mathbf{B} , while also nulling any background field.

A custom-built external-cavity diode laser (ECDL) [14] provides a stable, narrow-linewidth (≤ 3 MHz) 894 nm pump beam of up to 20 mW, which is expanded to be roughly circular with a diameter of 1 cm. The linearly polarized pump beam passes through a half-wave plate to allow rotation of the pump linear polarization vector ϵ to any angle

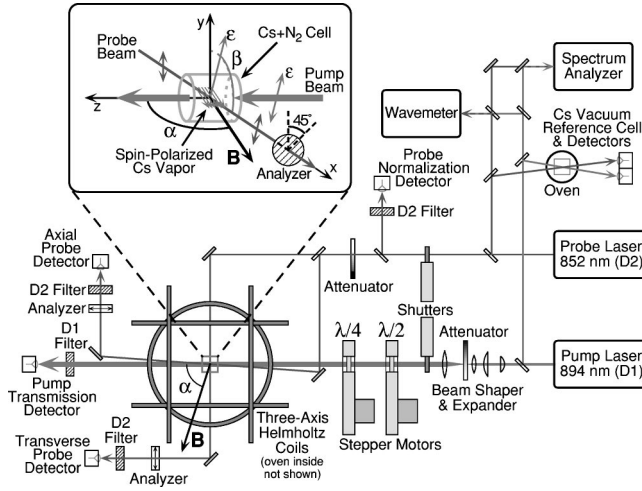


FIG. 4. Diagram of the experimental apparatus, with inset showing the setup of laser beams and fields at the Cs cell.

β relative to the x axis. The relationship between the various angles α , β , and θ (the true angle between the linear polarization vector of the pump light and the magnetic field) is given by $\cos \theta = \sin \alpha \cos \beta$. Thus for any magnetic-field angle α , when $\beta = 90^\circ$ then θ is also 90° , but when $\beta = 0^\circ$, then θ is small but nonzero ($\theta = 90^\circ - \alpha$). Following the half-wave plate, a quarter-wave plate (QWP) produces any degree of circular polarization along \mathbf{B} , given by $\cos \alpha \sin(2\phi)$, where ϕ is the angle between the fast axis of the QWP and the incident linear polarization.

An 852 nm ECDL provides the weak linearly polarized probe beam, which is detuned by several GHz from the $F=4$ components of the $D2$ line and attenuated to a few μW to avoid producing any optical pumping of its own. Optical rotation of the plane of polarization of this beam due to paramagnetic Faraday rotation acts as a measure of the ground-state spin polarization. For probe detunings $\Delta\nu_F$ (relative to each ground-state hyperfine component) which are large relative to the pressure-broadened linewidth, the rotation angle is given by [15,13]

$$\begin{aligned} \Phi_R &= \frac{NL\sigma_0}{2\pi} \left(\frac{11-4J(J+1)}{4} \right) \sum_F (-1)^F \frac{\langle m_F \rangle}{F\Delta\nu_F} \sin \alpha \\ &= \frac{NL\sigma_0}{2\pi} \left(\frac{\langle m_3 \rangle}{3\Delta\nu_3} - \frac{\langle m_4 \rangle}{4\Delta\nu_4} \right) \sin \alpha, \end{aligned} \quad (13)$$

where N is the cesium number density, L is the path length through the cell, and $\sigma_0 = \pi c r_e f$ (f is the oscillator strength of the probe transition). This rotation angle is measured by transmission through an analyzing polarizer set at 45° to the input polarization, producing a signal proportional to $\cos^2(\Phi_R - 45^\circ)$ which is the actual experimental observable.

The probe beam is split into an axial probe beam which propagates nearly parallel ($< 1^\circ$) to the pump beam and a transverse probe beam directed at 90° to the pump beam, to allow maximum sensitivity to the atomic polarization regardless of the magnitude of the field angle α . In practice, most of the useful data is taken with the transverse probe, since α

is typically set to around 80° . Photodiode detectors, with laser-line interference filters to block stray light, record the two probe beams and the transmitted pump light. A separate detector records a portion of the probe beam split off before entering the cell, in order to normalize any probe intensity fluctuations. At intervals during data taking, the wavelength and single-mode quality of the pump and probe lasers are monitored using a Michelson-interferometer wavemeter and a scanning Fabry-Perot optical spectrum analyzer. In addition, both beams are monitored through a separate Cs vacuum cell, to provide a reference absorption spectrum for frequency calibration.

All data channels are recorded by 12-bit analog-to-digital converters. During a data-taking sequence, the frequency and polarization state of the pump beam are controlled from a computer. The injection current and diffraction grating angle of the 894 nm ECDL are related quadratically and controlled by digital-to-analog outputs [14], allowing a continuous pump tuning range of up to 25 GHz. The angles of the half-wave and quarter-wave retardation plates are adjusted by computer-controlled stepper motors with a step size of 0.9° , thus setting the pump polarization state. In addition, computer-controlled mechanical shutters can be used to block the pump or probe beams, in order to subtract out detector offsets (for probe intensity normalization) and to allow turning off the pump light (so that the Cs atoms can depolarize) without turning off the laser.

V. EXPERIMENTAL DATA

The data sets consist primarily of hysteresis curves produced as the circular polarization of the pump light is varied about zero. The hysteresis curves are generated by setting the pump linear polarization angle β , and then sweeping the QWP from -45° to $+45^\circ$ and back to -45° relative to this angle, thus varying the pump polarization from fully right-circular through linear to fully left-circular and back again. The time between the 0.9° QWP steps is about 0.5 sec, to allow the atomic spin polarization to reach equilibrium at each step.

A complete set of hysteresis curves for a given pressure and temperature is typically taken at several laser tunings separated by about 400 MHz across the range of interest, with \mathbf{B} at $\alpha = 84^\circ$ relative to the pump beam and linear polarization angles $\beta = 0^\circ, 18^\circ, \dots, 90^\circ$. A portion of such a data set is shown in Fig. 5. Curves with $\beta = 90^\circ$ (light gray; linear polarization perpendicular to \mathbf{B} , so that $\theta = 90^\circ$) show spontaneous polarization and hysteresis across nearly the full broadened width of the $3 \rightarrow 4$ transition, while curves with $\beta = 0^\circ$ (dark gray; linear polarization nearly parallel to \mathbf{B} , with $\theta \approx 6^\circ$) reveal spontaneous polarization over a narrower range on the low-frequency side of the $3 \rightarrow 3$ transition.

Spontaneous polarization strong enough to produce hysteresis has been observed over wide ranges of buffer gas pressures, cell temperatures, and pump laser tunings, polarization angles, and intensities. Typical hysteresis curves for a range of N_2 pressures are shown earlier in Fig. 1. The maximum atomic spin polarization \mathcal{M} occurs at $\phi = 0^\circ$ (linearly polarized light), and for the 75 torr curve approaches the

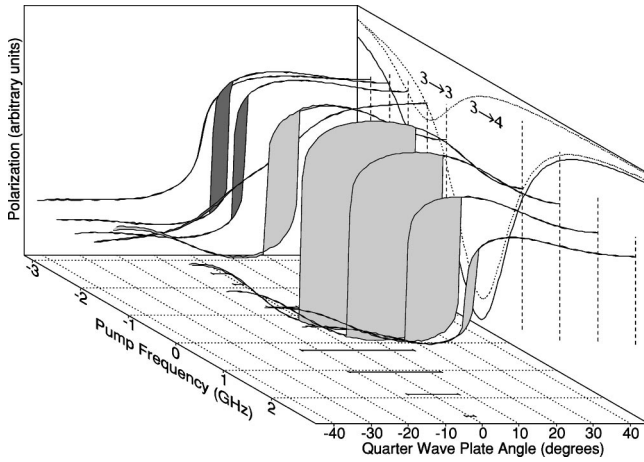


FIG. 5. Experimental data showing hysteresis curves as a function of pump detuning, at 100°C with 75 torr N_2 buffer gas. Light gray data taken at $\beta = 90^\circ$, dark gray at $\beta = 0^\circ$. An absorption spectrum and the hysteresis amplitudes are projected on the right plane of the 3D box, and the hysteresis widths on the bottom plane.

absolute maximum of $\mathcal{M}=4$. The strength of spontaneous polarization steadily decreases at higher N_2 pressure. Above 450 torr, the collisional broadening of the $D1$ line becomes comparable to the 9 GHz ground-state hyperfine splitting, and selective pumping of the $F=3$ level is no longer possible.

Spontaneous polarization has been observed at temperatures from $60\text{--}120^\circ\text{C}$, corresponding to number densities of 10^{12} cm^{-3} to $5 \times 10^{13}\text{ cm}^{-3}$ and spin exchange rates of $600\text{--}30000\text{ s}^{-1}$. The lowest threshold temperature for hysteresis has been about 62°C for the 75 torr cell, increasing to 80°C at 20 torr and to nearly 115°C at 450 torr. Hysteresis has been seen on both the $3 \rightarrow 3$ and $3 \rightarrow 4$ transitions from 20 to 75 torr, while in the higher-pressure cells (160 to 450 torr) it has occurred only on the $3 \rightarrow 4$. At 46 and 75 torr, hysteresis on the $3 \rightarrow 3$ transition has been seen over a range of about 1 GHz in frequency and for polarization angles $0^\circ \leq \beta < 36^\circ$. The stronger hysteresis on the $3 \rightarrow 4$ has been seen across nearly 4 GHz, for angles $54^\circ < \beta \leq 90^\circ$ at these two pressures. At higher pressures, the frequency range of observed spontaneous polarization on the $3 \rightarrow 4$ transition increases, up to 5 GHz at 300 torr, while the angular range is reduced somewhat to about $72^\circ < \beta \leq 90^\circ$. The pump intensities needed to achieve spontaneous polarization have varied from less than 0.5 mW/cm^2 in the most favorable regions at 75 torr and 70°C (corresponding to a pump rate on the $3 \rightarrow 4$ transition of 200 s^{-1}), to over 20 mW/cm^2 at 450 torr and 115°C . These observations are all in good agreement with the predictions of the theoretical model, including the threshold conditions for temperature and pump power and also the ranges of buffer gas pressure and polarization angles over which spontaneous polarization should occur.

In addition to generating hysteresis curves, time-evolution data can also be taken, by unblocking the pump beam with the shutter and then observing the atomic spin polarization as it grows to a stable, nonzero value (Fig. 6). This type of scan is useful for detecting spontaneous polarization in regions

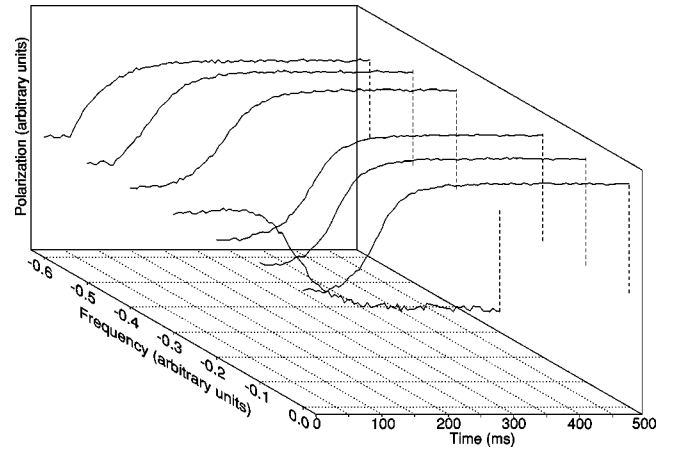


FIG. 6. Experimental time evolution data showing the spin polarization growing spontaneously from zero to a stable value after unblocking the pump beam at $t=0$. Note the bistable nature of the phenomenon, whereby the atomic ensemble may develop into either of the two bistable spin-polarized states during repeated trials. These data were taken at 82°C with 46 torr N_2 buffer gas, over a small frequency region centered on the $3 \rightarrow 4$ transition with $\beta = 90^\circ$.

where it is too weak to cause a large and easily visible hysteresis as the circularity is varied, and also for observing the spontaneous, bistable nature of the phenomenon. During repeated time-evolution scans under identical experimental conditions, the atomic ensemble may develop into either of the two bistable spin-polarized states, as seen in the data of Fig. 6 despite a small bias favoring one of the bistable states. By adjusting systematic biases (most importantly the residual circularity of the pump light and also stray magnetic fields), we have at times been able to produce a nearly even split in the direction of spin polarization over repeated trials. With more refined control over drifts in the bias, it should be possible to observe spontaneous polarization arising from statistical fluctuations alone.

VI. COMPARISON OF DATA AND MODEL

The theoretical model discussed in Sec. III is implemented using a computer program in which we numerically integrate the differential equations to find the time evolution of the ground-state density matrix. This program uses a standard fifth-order Runge-Kutta integration with adaptive step-size control. Appropriate values for the experimental parameters are entered, and the program then calculates all rates and coefficients using standard values for the cross sections and other constants.

To generate hysteresis curves which can be compared to the experimental data, the program starts with a small initial polarization bias and linearly polarized pump light. The spin polarization is allowed to grow to equilibrium, and then the pump polarization is stepped progressively towards full circular polarization, then back through linear polarization to the opposite sense of circular polarization. At each step, the model generates the equilibrium populations ρ_{Fm} , which can be summed to give the spin polarization $\langle m \rangle = \langle m \rangle_4 + \langle m \rangle_3$

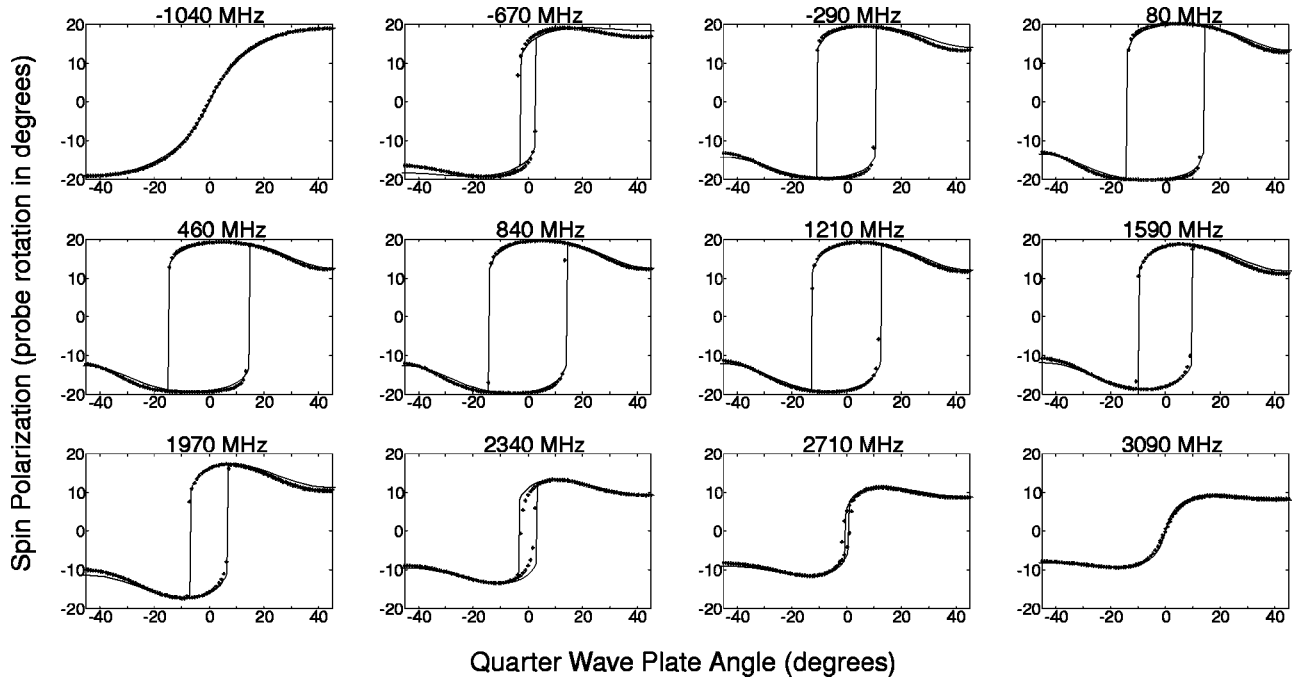


FIG. 7. Comparison of data (points) and model (solid lines) as a function of pump detuning relative to the $3 \rightarrow 4$ transition, at 85°C with 75 torr N_2 buffer gas and $\beta=90^\circ$. The data points overlap many portions of the model curves. All parameters except pump detuning are the same for all curves shown.

and also the optical rotation [Eq. (13)]. Once the vertical axis of the data is linearized, by correcting for the sinusoidal response of the analyzing polarizer, the hysteresis curves generated by experiment and model can be compared directly.

An array of such comparisons at 85°C with 75 torr N_2 buffer gas is displayed in Fig. 7, where the data and model are shown superimposed for each of 12 pump laser detunings spanning a 4 GHz range across the $3 \rightarrow 4$ transition. With a pump intensity of 4 mW/cm^2 , the rate of optical pumping on unpolarized atoms in the $F=3$ hyperfine level (at the $3 \rightarrow 4$ transition resonance) is about 2000 s^{-1} . Under these conditions of temperature and buffer gas pressure, the spin exchange rate is 4000 s^{-1} , the collisional electron spin-relaxation rate (γ_R) is 150 s^{-1} , and the effective electron spin-relaxation rate due to diffusion (γ_D) is about 250 s^{-1} (which has considerable uncertainty due to the optical pumping geometry). All rates are calculated using cross sections from Refs. [8–10]. The total calculated spin-relaxation rate is in reasonable agreement with our measurements using a variant of the standard “relaxation in the dark” technique [16].

We see no evidence of significant collisional spin relaxation in the $6P_{1/2}$ excited state itself. Large cross sections for spin relaxation (comparable to the quenching cross section) of $P_{1/2}$ states in Rb-N_2 collisions have been reported in Ref. [11], but our theoretical model fits the data well only if this excited-state spin relaxation is small (comparable to that expected from the transfer cross section of 5 \AA^2 mentioned earlier in Sec. II) or zero. Thus our data rule out such large depolarization cross sections for the cesium $6P_{1/2}$ state.

A single free parameter, an additional spin-relaxation rate γ_C , is included in the model to account for uncertainty in the

ground-state spin relaxation. We find broad general agreement across the frequency range shown in Fig. 7 even when this term is set to zero, but the best fit to the hysteresis curves is found for $\gamma_C=220 \text{ s}^{-1}$. This value indicates an uncertainty in the model as large as half the known ground-state spin relaxation, but it is nevertheless much smaller than the dominant rates (optical pumping and spin exchange). With this single value of γ_C used in all of the curves in Fig. 7, the hysteresis widths in data and model are seen to agree quite well over the entire frequency range, and the model also quantitatively reproduces most other aspects of the data curves.

VII. CONCLUSION

We have investigated in detail the phenomenon of spontaneous polarization in cesium vapor under a broad range of experimental conditions. We have observed the spontaneous growth of spin polarization into either of the two stable spin directions, parallel or anti-parallel to the magnetic field, and we have measured hysteresis curves of spin polarization versus the circular polarization of the pump light.

In conjunction with the experimental work, we have developed a detailed theory of spontaneous polarization. Our density-matrix theoretical model includes the effects of coherence in the excited state, and the predictions of this model agree well with experimental observations. Using this model one can investigate other possibilities, including the behavior of spontaneous polarization under isotropic optical pumping and at very low magnetic fields. Under conditions where spontaneous polarization has been observed over wide ranges of the angle θ , isotropic pumping with unpolarized

light could open the possibility of continuously pumped spin precession, whereby atoms precessing about a weak magnetic field would have their spin polarization reinforced regardless of the polarization orientation. One can also investigate the possibility of observing spontaneous polarization in other alkalis, such as rubidium, or in optically pumped solids such as semiconductors [3,17].

ACKNOWLEDGMENTS

We thank Alex Cronin and Travis Norsen for assistance in constructing portions of the experimental apparatus, and Wolf Ketter for work on early versions of the modeling code. This project is supported by National Science Foundation Grant Nos. PHY-9732513 and PHY-0099535.

-
- [1] N. Fortson and B. Heckel, *Phys. Rev. Lett.* **59**, 1281 (1987).
 [2] W. M. Klipstein, S. K. Lamoreaux, and E. N. Fortson, *Phys. Rev. Lett.* **76**, 2266 (1996).
 [3] M. I. Dyakonov and V. I. Perel, *Pis'ma Zh. Éksp. Teor. Fiz.* **16**, 563 (1972) [*JETP Lett.* **16**, 398 (1972)].
 [4] A. Andalkar and R. B. Warrington, *Phys. Rev. A* (to be published).
 [5] D. A. McGillis and L. Krause, *Can. J. Phys.* **46**, 1051 (1968).
 [6] W. Happer, *Rev. Mod. Phys.* **44**, 169 (1972).
 [7] F. A. Franz, R. Boggy, and C. E. Sooriamoorathi, *Phys. Rev. A* **11**, 1 (1975).
 [8] N. D. Bhaskar, J. Pietras, J. Camparo, W. Happer, and J. Liran, *Phys. Rev. Lett.* **44**, 930 (1980).
 [9] F. A. Franz and C. E. Sooriamoorathi, *Phys. Rev. A* **10**, 126 (1974).
 [10] J. Vanier and C. Audoin, *The Quantum Physics of Atomic Frequency Standards* (Adam Hilger, Philadelphia, 1989).
 [11] A. Sieradzan and F. A. Franz, *Phys. Rev. A* **25**, 2985 (1982).
 [12] B. S. Mathur, H. Y. Tang, and W. Happer, *Phys. Rev. A* **2**, 648 (1970).
 [13] W. Happer and B. Mathur, *Phys. Rev.* **163**, 12 (1967).
 [14] A. Andalkar, S. K. Lamoreaux, and R. B. Warrington, *Rev. Sci. Instrum.* **71**, 4029 (2000).
 [15] W. Happer and B. Mathur, *Phys. Rev. Lett.* **18**, 577 (1967).
 [16] W. Franzen, *Phys. Rev.* **115**, 850 (1959).
 [17] D. D. Awschalom and J. M. Kikkawa, *Phys. Today* **52**(6), 33 (1999). J. M. Kikkawa, I. P. Smorchkova, N. Samarth, and D. D. Awschalom, *Science* **277**, 1284 (1997).